Published in final edited form as:
Mol Genet Metab. 2009 December ; 98(4): 356–366. doi:10.1016/j.ymgme.2009.06.016.

Developmental Expression Pattern of the Cholesterogenic Enzyme NSDHL and Negative Selection of NSDHL-deficient Cells in the Heterozygous *Bpa*^{1H}/+ Mouse

David Cunningham[a,b,*], **Kaitlyn Spychala**[a], **Keith W. McLarren**[c], **Luis A. Garza**[d], **Cornelius F. Boerkoel**[c], and **Gail E. Herman**[a,b]

[a]The Research Institute at Nationwide Children's Hospital, Columbus, OH 43205, USA

[b]Department of Pediatrics, The Ohio State University, Columbus, OH 43205, USA

[c]Provincial Medical Genetics Programme, Department of Medical Genetics, University of British Columbia, Vancouver, Canada

[d]Department of Dermatology, Johns Hopkins School of Medicine, Baltimore, MD 21287, USA

Abstract

NSDHL (NAD(P)H sterol dehydrogenase-like), is a 3β-hydroxysterol dehydrogenase thought to function in the demethylation of sterol precursors in one of the later steps of cholesterol biosynthesis. Mutations in the X-linked *NSDHL* gene cause CHILD syndrome in humans, and the male-lethal bare patches (*Bpa*) phenotype in mice. The relative level of NSDHL expression among different mouse tissues at several stages of embryogenesis and postnatal development was analyzed by immunohistochemistry. In wild type (WT) embryos, the highest levels of expression were seen in the liver, dorsal root ganglia, central nervous system, retina, adrenal gland and testis. Heterozygous *Bpa*^{1H} females are mosaic for NSDHL expression due to normal random X inactivation. NSDHL deficient cells were detected in the developing cerebral cortex and retina of *Bpa*^{1H} female embryos. In postnatal WT and *Bpa*^{1H} animals, we compared the expression pattern of NSDHL in skin, an affected tissue; liver, a main site of cholesterol synthesis; and brain, a tissue dependent on endogenous synthesis of cholesterol due to lack of transport across the blood-brain barrier. Clonal populations of mutant cells were visible in the brain, skin and liver of *Bpa*^{1H} pups. In the liver, the proportion of NSDHL negative cells dropped from ~50% at postnatal day 6 to ~20% at one year of age. In the brain, which showed the highest expression in cerebral cortical and hippocampal neurons, the proportion of NSDHL negative cells also dropped dramatically over the first year of life. Our results suggest that while NSDHL deficient cells in the mosaic *Bpa*^{1H} female are able to survive and differentiate during embryonic development, they are subject to negative selection over the life of the animal.

*Corresponding author. Address: The Research Institute at Nationwide Children's Hospital, 700 Children's Drive, Rm W470, Columbus, OH 43205, USA., FAX: +1 614 722 2817, E-mail address: David.Cunningham@nationwidechildrens.org.

Introduction

Cholesterol is an essential lipid component of animal cell membranes where it affects membrane fluidity. It is enriched in structural domains, such as lipid rafts and caveolae, that influence the localization and trafficking of membrane-bound proteins [1]. Cholesterol homeostasis is mediated through a combination of endogenous biosynthesis and dietary uptake, along with lipid binding proteins and receptors that mediate its transport, storage, catabolism and excretion [2]. The cholesterol biosynthetic pathway involves approximately 20 enzymes, with HMG-CoA reductase (HMGCR) catalyzing the rate-limiting, first committed step. Intermediate molecules in the pathway provide precursors for a variety of other cellular processes, including the prenylation of proteins and the synthesis of heme A, dolichol, vitamin D and oxysterols. Moreover, cholesterol is itself a precursor for the synthesis of steroid hormones and neurosteroids. Finally, the covalent binding of cholesterol to hedgehog proteins, a family of secreted, signaling morphogens with a broad range of functions in development, affects their localization and physical range of activity [3].

Studies of mouse mutants show that the phenotypes resulting from loss of function of cholesterogenic enzymes vary in severity depending on the step of the pathway that is affected, with defects in earlier steps giving more severe phenotypes than those at later steps. For example, loss of HMGCR activity results in early embryonic lethality around the time of implantation, while mutants lacking 7-dehyrocholesterol reductase (DHCR7), the last enzyme of the pathway, die within the first days after birth [4–6]. This trend is also reflected in humans by a range of defects seen in patients with inherited disorders of cholesterol synthesis [7–9].

NSDHL (NAD(P)H sterol dehydrogenase-like) is a 3β-hydroxysterol dehydrogenase that is thought to function in C-4 demethylation of sterol intermediates in one of the later steps of the cholesterol biosynthetic pathway [10]. The enzyme is localized to membranes of the endoplasmic reticulum (ER) and the surface of lipid droplets [11]. Mutations in the X-linked *Nsdhl* gene are responsible for the phenotype of the bare patches (*Bpa*) and striated (*Str*) mouse lines [10]. The Bpa^{1H} allele of *Nsdhl* is defined by a K103X nonsense mutation that is thought to abolish the enzymatic activity and disrupt the normal subcellular localization of the protein (Liu et al 1999; Caldas and Herman, 2003). A majority of affected Bpa^{1H} males die between E7.5 and E9.5, typically displaying grossly abnormal morphology [12,13]. Heterozygous Bpa^{1H} females are mosaic for the expression of WT and mutant NSDHL due to random X inactivation. The hallmark of affected females is the development hyperkeratotic eruptions in the skin at postnatal day 5 that resolve to hairless patches after 2–3 weeks [14]. They also display skeletal defects, occasional microphthalmia, and, on average, are smaller than wild type (WT) littermates at birth [15]. Mutations in the human *NSDHL* gene cause CHILD syndrome, a rare disorder causing early embryonic lethality in males, and unilateral skin defects and limb reduction in females [16–18].

In light of the early embryonic lethality of Bpa^{1H} males, we wondered about the fate of Bpa^{1H} cells in the mosaic female. Here, we present results from an investigation of the expression pattern of NSDHL in WT mice and Bpa^{1H} females. We used immunohistochemistry to identify NSDHL positive cell types in selected WT tissues, and then asked whether a population of NSDHL negative cells survived in the same tissues in Bpa^{1H} females. We focused on three organs: the liver, because it is a primary site of cholesterol biosynthesis in the body; the skin, because of its striking phenotype in Bpa^{1H} females; and the brain, because of its relatively high cholesterol content and the fact that it is entirely dependent on endogenous cholesterol biosynthesis due to the blood-brain barrier [19]. We found that NSDHL negative cells survive in the Bpa^{1H} mosaic female through embryonic and neonatal development, but that they are then subject to negative selection over the lifetime of the animal.

Material and Methods

Mice and Cells

A breeding stock of *Bpa*^{1H} mice [12] was maintained by mating heterozygous *Bpa*^{1H} females to F1 hybrid C57BL/6JA$^{w\text{-}J}$ X CBA/CaGnLe (B6CBA) males (The Jackson Laboratory, Bar Harbor, ME). Mice were fed our routine institutional high-fat chow, with no cholesterol (Harlan Teklad Rodent Diet 2919). *Bpa*^{1H} and WT mouse embryonic fibroblasts (MEFs) were cultured as previously described [20]. Embryos were genotyped for sex and the *Bpa*^{1H} allele by PCR analysis of yolk sac DNA as previously described [21,22]. All procedures involving mice conformed to protocols approved by the Institutional Animal Care and Use Committee of the Research Institute at Nationwide Children's Hospital.

Antibodies

A rabbit polyclonal antiserum was generated using the peptide antigen DEAVERTVQSFHHLRKDK corresponding to amino acid residues 345–362 of mouse NSDHL (Genemed Synthesis, San Francisco, CA). Anti-NSDHL antibodies were purified from the rabbit serum using a SulfoLink kit (Pierce, Rockford, IL) according to the manufacturer's protocol. Phospho-histone H3 (PHH3) was detected in immunohistochemistry experiments using a rabbit polyclonal anti-PHH3 antibody (Cell Signaling Technology, Danvers, MA). β-tubulin was detected on immunoblots using rabbit polyclonal anti-β-tubulin antibodies (catalog number RB-9249-P0, Thermo Scientific, Fremont, CA).

Immunoblot analysis

For protein extracts, mouse embryonic fibroblasts were lysed and tissues were homogenized in RIPA buffer (150 mM NaCl, 10 mM Tris pH 7.2, 0.1% SDS, 1% Triton X-100, 1% deoxycholate, 5 mM EDTA). Protein concentration in the lysates was measured using the BCA Protein Assay Kit (Pierce, Rockford, IL). Proteins were resolved by SDS-PAGE and transferred to Hybond ECL membrane as previously described [11]. Preblocking, primary antibody binding and secondary antibody binding to immunoblots were carried out in TBST (10 mM Tris pH 7.0, 150 mM NaCl, 0.1% Tween-20) with 2% normal goat serum. The secondary antibody was HRP-linked anti-rabbit IgG (Cell Signaling, Danvers, MA). Antibody binding was visualized using SuperSignal West Pico Chemiluminescent Substrate (Pierce, Rockford, IL) and exposing the blots to X-Omat film (Kodak, Rochester, NY).

Immunohistochemistry

Mouse embryos and adult tissues were fixed overnight at 4° C in Bouin's fixative and rinsed in 70% ethanol. Adult brains were fixed by transcardial whole-animal perfusion with Bouin's fixative. Fixed tissues were embedded in paraffin blocks and sectioned at a thickness of 5 μm. After deparaffinization, slides were heated to 95° C for 20 min in antigen retrieval solution (10 mM sodium citrate, 0.05% Tween-20, pH 6). Slides were incubated with Peroxidase Blocking Reagent, Protein Block and primary antibody diluted to 1:500 in Antibody Diluent (Dako, Carpinteria, CA) according to the manufacturer's instructions. Primary antibody binding was amplified using a Vectastain Elite ABC kit (Vector Laboratories, Burlingame, CA), including biotinylated anti-rabbit secondary antibody. Antibody binding was visualized using the Liquid DAB+ Substrate Chromogen System (Dako, Carpinteria, CA). Samples were counterstained for 1 min with hematoxylin. Photomicrographs were acquired with SPOT version 3.5 software operating SPOT RT Color digital cameras (Diagnostic Instruments, Sterling Heights, MI) mounted on a Nikon SMZ-10A microscope or a Nikon Eclipse E800 microscope. No adjustments were made in the color, contrast or hue of the photomicrographs. In experiments where the ratio of NSDHL stained vs unstained hepatocytes was measured and compared at

different ages, statistically significant differences from the expected 1:1 ratio were determined using a one-sample t test.

Results

Generation of a specific anti-NSDHL polyclonal antibody

A rabbit polyclonal antiserum was raised against a peptide corresponding to the 18 amino acids at the carboxy-terminus of the mouse NSDHL protein. Anti-NSDHL antibodies were affinity purified from the antiserum using the peptide immunogen and tested for specificity by immunoblotting (Fig. 1). Mouse NSDHL comprises 362 amino acids with a predicted molecular mass of 38 kD. A single band near the expected position on the blot was detected in a whole-cell lysate from WT MEFs. A lysate from *Bpa*^{1H} MEFs served as a negative control. The truncated peptide that is predicted to be encoded by the *Bpa*^{1H} allele lacks the carboxy-terminal region of NSDHL, and was not detected by our antibody (Fig. 1, lane 2). A replicate blot that was probed with an anti-β-tubulin antibody demonstrated equivalent protein concentration and integrity of the WT and *Bpa*^{1H} MEF samples (Fig. 1, lower panel). The NSDHL antibody showed highly specific staining in total protein extracts from WT E16.5 embryo, adult liver and adult brain. A relatively faint band seen in the liver extract that migrated slightly faster than the 38 kD NSDHL band may be either a partial degradation product of NSDHL or nonspecific binding to another protein. However, since it represented a small proportion of the total signal in the sample, we concluded that the antibody would provide an informative reagent for immunohistochemical analysis of NSDHL expression in WT tissues, as well as distinguishing WT and mutant cells in mosaic *Bpa*^{1H} female mice. The lack of detectable signal for β-tubulin in the liver extract is due, in part, to the relatively low level of tubulin expression in this tissue [23]. Faint β-tubulin signal was detected in this sample when loading was increased to 40 μg (not shown).

Embryonic expression pattern

In crosses between heterozygous *Bpa*^{1H} females and WT males, 25% of the embryos are expected to be hemizygous *Bpa*^{1H} males. In six litters of E7.5 embryos from this cross, we found 23% (9 out of 38) were *Bpa*^{1H} males. No viable male *Bpa*^{1H} embryos are found at E11.5 [13]. These data suggest that NSDHL is not required for preimplantation viability, but is essential for normal development around the time of gastrulation. NSDHL staining of WT embryos at E6.5 and E7.5 resulted in a relatively low and uniform level of signal throughout all cell-types (Supplemental Fig. 1). In E8.5 embryos, cells of the developing neural tube showed distinctly higher expression than those in other tissues (not shown). An increasingly complex expression pattern in the developing central nervous system (CNS) and peripheral neurons was evident in E10.5 embryos (Fig. 2A). Notably, the dorsal root ganglia (DRG) and differentiating motor neurons in the basal (ventral) column of the neural tube demonstrated intense staining (Fig. 2B, D). Strong expression of NSDHL was also detected in a subset of cells within the fetal liver (Fig. 2C). Since cholesterol is an essential component of the plasma membrane, we asked whether high NSDHL expression was associated with highly proliferative cells by staining with an anti-phosphorylated histone H3 (PHH3) antibody that detects mitotic cells. In the neural tube, numerous mitotic cells were seen in the ventricular layer, as expected. Few, if any PHH3 positive cells were seen in the differentiating neurons of the basal column that showed higher NSDHL expression (Fig. 2E, arrow). Thus, while NSDHL staining was present in dividing cells of the neurepithelium, a substantially higher signal was seen in specific subsets of differentiating neurons.

In the E14.5 embryo, NSDHL expression was again prominent in the liver, DRG and the developing brain (Fig. 2F). The trigeminal ganglion and superior cervical ganglion also showed very high levels of NSDHL. In addition, the adrenal gland and Leydig cells of the testis, both

of which are highly steroidogenic cell types, were intensely stained (Fig. 2G, Supplemental Fig. 2). Metanephric glomeruli and epithelial cells of metanephric tubules in the kidney, as well as epithelial cells of the intestine, showed moderately high levels of NSDHL. Strong expression was also seen in a layer of condensing mesenchyme surrounding developing ribs, specifically in the dorsal/caudal region of the embryo (Fig. 2H).

The pattern of NSDHL expression detected by immunostaining among tissues of the midgestation embryo was supported by in situ hybridization analysis of the E15.5 embryo using a radiolabeled antisense RNA probe that detected *Nsdhl* mRNA (Supplemental Fig. 3). High levels of *Nsdhl* transcripts were detected in the liver, brain, adrenal, cranial ganglia, and intestinal epithelium.

Since a Bpa^{1H} heterozygous female would be expected to show mosaic NSDHL expression due to random X inactivation, we compared the staining pattern in the neopallial cortex (developing cerebral cortex) of a WT E14.5 embryo with that of a mutant embryo (Fig. 2I, J). The WT embryo showed a continuous band of stained neurons throughout the cortex, including evidence of signal in the dendrites of neurons (Fig. 2I). In the mutant embryo, patchy staining arranged in sectors that radiated out from the ventricular layer was present throughout the cortex (Fig. 2J). This pattern is consistent with a mixed population of WT and mutant progenitor cells in the ventricular layer giving rise to clonal populations of differentiating neurons that migrate away from the ventricle to populate the developing cerebral cortex.

A pattern similar to that found in the mutant neopallial cortex was seen in the embryonic retina. At E15.5, the WT eye showed strong staining for NSDHL in the ganglion cell layer (GCL), with lower signal throughout the neuroblast layer (NL) of the developing retina (Fig. 2K). This pattern was confirmed by in situ hybridization analysis that showed high levels of *Nsdhl* mRNA in the retina at E15.5. The GCL comprises proliferating stem cells that give rise to all neural cell types of the mature retina. In the Bpa^{1H} female eye, the GCL included both NSDHL positive and negative cells (Fig. 2L). The differentiating cells of the NL showed sectors of stained and unstained cells radiating out from the GCL. These results demonstrate that mutant neural progenitor cells present in the fetal brain and eye give rise to differentiating neurons and that they migrate to the appropriate position in the developing tissue.

Liver

The mature liver is composed of structural subunits called lobules, defined primarily by the arrangement of their vasculature. Portal veins arranged in a ring transport blood into the lobule where it flows through sinusoids between cords of hepatocytes and drains into a central vein that carries blood out of the lobule. In the adult WT liver, staining for NSDHL produced strong signal in all hepatocytes. A slight zonal gradient of expression was evident, with the highest levels in the pericentral region of lobules (Fig. 3A). In livers from Bpa^{1H} females over one year of age (13–14 mo), a mosaic pattern of staining in hepatocytes was observed (Fig. 3B, C, D).

In the absence of selective pressure, WT and mutant cells would be expected to be present in roughly equal numbers due to random X-inactivation in early embryogenesis. However, a majority of hepatocytes were NSDHL positive in livers from adult Bpa^{1H} females (Fig. 3B), with small clusters of unstained cells clearly distinguishable (Fig. 3C). To quantitate this skewed ratio, at least 1500 hepatocytes were scored as either NSDHL positive or negative in livers from 12 Bpa^{1H} females over 1 year of age (13–14 mo). The mean percentage of WT hepatocytes in the 12 samples was 79 (SD: 10), significantly higher than the expected 50% ($p<0.0001$). In the affected livers that showed the highest (~40%) proportion of unstained hepatocytes (Fig. 3D), a nonrandom pattern of positive and negative hepatocytes was observed, with stained cells highly concentrated in pericentral region of the lobules (Fig. 3D). These

results suggest that *Bpa*^{1H} hepatocytes undergo negative selection in affected females, either due to a lower proliferation rate or increased cell death. Furthermore, this effect appears to depend, in part, on their position within the lobule.

Since NSDHL is expressed strongly in hepatocytes from early fetal stages through adulthood, we asked at what developmental stage the proportion of WT to mutant cells begins to deviate from the expected 1:1 ratio and show a nonrandom distribution in the liver. Staining of livers from P6 *Bpa*^{1H} females revealed an apparently random distribution of positive and negative cells (Fig. 3E). The average percentage of NSDHL positive hepatocytes in livers from six *Bpa*^{1H} P6 females was 52 (SD: 5). Among six mutant livers at P25, the average percentage of NSDHL positive hepatocytes increased to 62 (SD: 9). However, in contrast to the older livers, their distribution appeared to be nearly random throughout the lobules (Fig. 3F). Thus, the ratio of WT to mutant cells at P6 (52%) was not significantly different from the expected 1:1 ($p=0.33$). In P25 livers, the proportion of WT hepatocytes (62%) was significantly higher than 50% ($p=0.017$). These data suggest that the higher percentage of WT hepatocytes present in livers from older *Bpa*^{1H} females is the cumulative result of postnatal differences in either the growth rate or survival of WT vs mutant hepatocytes.

Skin

In normal development, the onset of hair follicle development is marked by the induction of epidermal placodes at E14.5 [24]. Stratification and differentiation of the epidermis occurs between E14.5 and E18.5 [25]. In WT embryos at E16.5, NSDHL staining was visible in the outermost layer of the epidermis, with little or no staining in the developing hair follicles (Supplemental Fig. 4). Regions of NSDHL negative and positive skin were detected in *Bpa*^{1H} female embryos, consistent with the expected mosaic expression pattern. The NSDHL positive and negative areas in the *Bpa*^{1H} mosaic skin were histologically similar to each other and to that of entirely WT embryos (Supplemental Fig. 4).

In WT dorsal skin at P2, NSDHL expression showed a distinct pattern within the developing hair follicles (Fig. 4A). Staining was strongest in the sebaceous glands, with moderate staining also present in the matrix and inner root sheath. Staining was not observed in the outer root sheath at the level between the arrector pili muscle and the sebaceous gland, the hair follicle stem cell niche known as the bulge. Low level NSDHL expression was seen in the epidermis. In a *Bpa*^{1H} littermate, the epidermis and hair follicles appeared to be morphologically normal in regions that lacked NSDHL staining, indicating that hair follicle morphogenesis is not grossly abnormal in *Bpa*^{1H} mutant skin at this stage (Fig. 4B).

In WT dorsal skin at P6, when hair shafts had emerged from the follicles, NSDHL staining was very strong in the inner and outer root sheaths in the non-permanent segment of the hair follicle below the insertion of the arrector pili muscle, as well as the sebaceous glands (Fig. 4C, E). The mosaic expression of NSDHL was evident in skin from a *Bpa*^{1H} female littermate (Fig. 4D, F). A low magnification view of alternating regions of NSDHL positive and negative hair follicles revealed that a lack of NSDHL expression resulted in arrested downgrowth of the follicles, indicative of impaired progression through the anagen hair cycle within the mutant areas of skin (Fig. 4D). The mutant follicles were smaller and shorter than adjacent WT follicles and lacked hair shafts, consistent with defective anagen hair growth. A higher magnification view of an NSDHL negative region showed a thickened epidermis with cystic invaginations reminiscent of utricles, and a thickened dermis with inflammatory infiltrate (Fig. 4F). Hyperkeratotic material could be visualized in the cystic structures.

The bands of hyperkeratotic eruptions that characterize the skin of *Bpa*^{1H} females at 1 week of age resolve to narrow stripes of hairless skin after several weeks. In the dorsal skin from an 8 week old *Bpa*^{1H} female that showed relatively large stripes of affected skin, NSDHL staining

revealed clear domains of positive and negative tissue (Fig. 4G). In the positively stained regions, hair follicles showed strong staining in the inner and outer root sheaths below the arrector pili muscle as well as the matrix region of the hair bulb. Sebaceous glands were strongly positive and the epidermis was weakly positive for NSDHL, as in the skin from P2 and P6 pups. In the NSDHL negative skin, hair shafts were absent and the hair follicles appeared to be in the telogen stage of the hair cycle despite the predominance of anagen stage follicles in the adjacent WT skin. Although the majority of follicles in the mutant patches appeared to be in telogen, a few scattered deeper follicular units consistent with anagen follicles were observed. The sebaceous glands associated with the predominantly telogen follicles in the mutant regions appeared enlarged, similar to the phenotype of other mouse mutants that display sebaceous gland hyperplasia in the context of alopecia [26,27]. The general lack of anagen hair follicles in the mature *Bpa*^{1H} skin lesions resembled the phenotype seen in the P6 skin. The dermis in the mature affected skin was marked by the presence of amorphous debris that was noted in previous studies of *Bpa*^{1H} skin [14].

Brain

The cholesterol concentration of the adult mouse brain is about 7-fold higher than the average cholesterol concentration of the whole animal [19]. Because cholesterol is not transported across the blood-brain barrier, cholesterol biosynthesis within the brain is essential for its normal growth and development [28]. In the postnatal mouse, the rate of cholesterol synthesis in the CNS is highest (300–400 nmol/hr) during the first three weeks after birth, after which it drops about 6-fold and stabilizes at 10–13 weeks of age [29]. In light of the substantial age-dependent differences in rates of cholesterol biosynthesis, we first identified which cells express NSDHL in the WT brain during early postnatal development and in the adult. We then asked whether NSDHL negative cells were present in these cell populations in *Bpa*^{1H} mutant female pups and adults.

In WT brain at P2, the distribution of cells expressing NSDHL was complex, with at least some positive cells in virtually all regions. However, broad patterns of relatively high expression were evident. Staining was prominent in a wide band of differentiating neurons in the cortical plate of the cerebrum (Fig. 5A, C). As noted in developing neurons of the E14.5 embryo (Fig. 2I), the cell bodies as well as dendrites were stained. Pronounced NSDHL signal was also present in hippocampal neurons (Fig. 5E). In the cerebellum, staining was strongest in the layer of cells composed of Purkinjie cell precursors and Bergmann glia (not shown). Because Purkinjie cells do not display a fully differentiated morphology at P2, we were not able to determine whether one or both cell types are positive for NSDHL at this stage. Distinct staining was also seen in cells throughout the thalamus (Fig. 5E) and in the mitral layer neurons in the developing olfactory bulb (Fig. 5A, see arrow). Regions that showed relatively low staining included the intermediate cortical layer and subventricular layers of the cerebrum, the dentate gyrus, granular cells of the developing striatum (caudate putatem), granular cells of the olfactory bulb, the superior colliculus and the choroid plexus.

In the *Bpa*^{1H} female P2 brain, a mosaic pattern of NSDHL staining was most evident in the cerebrum and hippocampus (Fig. 5B, D, F). In the cerebrum, radiating sectors of NSDHL positive and negative neurons were visible in a pattern similar to that seen in the *Bpa*^{1H} E14.5 embryo (compare Fig. 2J and Fig. 5D). Likewise, the P2 mutant hippocampus was composed of a mixture of stained and unstained cells throughout its length (Fig. 5F), in contrast to the WT hippocampus that showed regions where virtually all of the cells were NSDHL positive (Fig. 5E). A similar pattern was observed in the hippocampus of WT and *Bpa*^{1H} female brains at P25 (Supplemental Fig. 5, Panels A–D). Although the overall intensity of NSDHL staining in hippocampal neurons was lower in P25 brains than P2 brains, the WT hippocampus was evenly stained throughout its length, while the *Bpa*^{1H} hippocampus was composed of both

stained and unstained neurons. These results suggest that a substantial number of NSDHL deficient neurons survive to birth in the *Bpa*^{1H} female, presumably acquiring cholesterol from WT neurons and/or glia.. We were not able to assess the extent of mosaicism in other regions of the *Bpa*^{1H} brain due to the heterogeneous levels of NSDHL staining seen among different cell types in these or the same regions of the WT brain.

The general pattern of NSDHL staining in the WT brain at 1 year of age resembled that of the P2 brain in that signal was most pronounced in the cerebral cortex and CA1 and CA3 regions of the hippocampus (Fig. 5G, I). This profile is in agreement with data provided in the Allen Brain Atlas for *Nsdhl* gene expression in the WT mouse brain using in situ hybridization analysis (http://www.brain-map.org). We also observed positive cells dispersed throughout white and gray matter, displaying a morphology consistent with glial cells. NSDHL staining in the adult brain differed from the neonatal brain in two major ways. First, overall, the proportion of strongly positive cells was lower in the adult. For example, in the adult cerebral cortex, a narrow layer of large pyramidal neurons showed distinct staining (Fig. 5G, arrow), in contrast to the much broader band of differentiating cortical neurons in the P2 brain (Fig. 5C). The relatively large size of the nuclei and cell bodies of these adult neurons, as well as their position, are consistent with layer V of the cerebral cortex. The second distinguishing feature of the adult brain, is that signal was visible mainly in the cell bodies of neurons, with much fainter staining in the dendrites (compare cortical neurons at P2, Fig. 5C, with adult cortical neurons, Fig. 5G).

At a gross level, the *Bpa*^{1H} adult brain was indistinguishable from the WT brain with regard to the pattern of NSDHL staining (Fig. 5H, J). No patches of unstained neurons were observed in the layer of NSDHL positive cortical neurons or in the CA1 and CA3 regions of the hippocampus, as was seen in the P2 *Bpa*^{1H} brain. Upon close examination, only a few NSDHL negative hippocampal neurons could be seen among the hundreds of positive cells within the CA1 and CA3 regions that were visible on each section (Supplemental Fig. 5F), suggesting that the mutant neurons are subject to negative selection over the life of the animal. Due to the wide variation in levels of NSDHL expression among neurons of the WT cerebrum, it was not possible to determine whether a small number of mutant cells were present among the positive cells in the *Bpa*^{1H} adult brain. This grossly WT pattern of NSDHL signal was present in brains from three *Bpa*^{1H} females at 1 year of age.

Discussion

While cholesterol biosynthesis is a fundamental housekeeping function shared by most, if not all, cell types, the activity level of the pathway varies widely among different tissues [30,31]. This variation may reflect different requirements for either functional intermediate molecules in the pathway, cholesterol itself, or cholesterol as a precursor for the synthesis of steroid hormones or neurosteroids. Analyses of the consequences of perturbing the pathway at various steps may allow these multiple functions to be distinguished. Because cholesterol can be acquired through dietary intake and transported via lipoproteins in the serum, a primary question in understanding the pathologies associated with disorders of cholesterol synthesis in humans is whether they result from cholesterol deficiency per se, a deficiency of key precursor molecules, or the abnormal accumulation of sterol intermediates to toxic levels due to a block in the pathway. Testing these hypotheses is complicated by the fact that sterol intermediates that share the greatest structural similarity to cholesterol, such as desmosterol and 7-DHC, can incorporate into cell membranes. However, substitution of cholesterol with desmosterol or 7DHC alters the physical properties of membranes, impairs lipid raft-dependent signaling, and alters the structure and function of caveolae [32–34]. This partial functional overlap with cholesterol probably accounts for the survival to birth of mouse embryos that are homozygous for null mutations in *Dhcr24* and *Dhcr7*, in contrast to the much earlier embryonic lethality of

mutations in enzymes such as squalene synthase and NSDHL that block earlier steps in the pathway [35,36].

Previously, we compared the survival of *Bpa*^{1H} vs WT cells in vitro by sorting and counting mutant and WT cells in primary cultures of MEFs from *Bpa*^{1H} female E15.5 embryos [20]. We found no evidence of negative selection acting on mutant cells in utero, since on average they were present in proportions equivalent to WT cells at the time they were isolated. In a mixed population of MEFs, the ratio of mutant to WT cells did not change significantly after nine passages in culture. Sorted populations of mutant and WT cells grew equally well in the presence of 10% normal fetal bovine serum. However, in the presence of delipidated serum, most of the cells in a pure *Bpa*^{1H} population died within 48 hrs. WT cells did not show cell death in delipidated serum. Finally, when cultured with WT MEFs in delipidated medium, the *Bpa*^{1H} cells showed no cell death after 48 hrs, suggesting that the mutant cells were rescued by presence of WT cells. Our analysis of heterozygous *Bpa*^{1H} female mice, that are randomly mosaic for WT and NSDHL deficient cells, allowed us to ask similar questions in vivo.

Varying levels of NSDHL expression among different cell types were apparent in WT E10.5 embryos with the highest signal found in the CNS, DRG and fetal liver. Within the CNS, differentiating motor neurons of the neural tube showed the most intense staining (Fig. 2F). The DRG of the peripheral nervous system were also strongly stained for NSDHL. These results are consistent with a previous study of the expression of cholesterogenic enzymes in the mouse embryo using whole-mount in situ hybridization, where strong *Nsdhl* mRNA expression was detected in the DRG and neural tube at E10.5 [37]. A reason for the relatively high CNS expression that was evident at this stage may be the formation of the blood-brain barrier. Maternally derived cholesterol accounts for a substantially lower proportion of the total cholesterol in the fetal brain than other fetal tissues after E10, as demonstrated by sterol measurements in *Dhcr7* −/− embryos and levels of isotopically labeled cholesterol injected into dams that was measured in fetal organs [38,39]. Further, the relatively high level of NSDHL that was observed particularly in differentiating neurons may be due, in part, to a requirement for cholesterol in the large amount of plasma membrane required for the growing dendrites and axons of these cells. Finally, neurons of the CNS and peripheral nervous system, including the DRG, trigeminal ganglion, superior cervical ganglion and ganglion cell layer of the retina, synthesize neurosteroids from cholesterol, as demonstrated by the expression and activity in these cells of P450scc, a mitochondrial enzyme that initiates the conversion of cholesterol to pregnenolone [40,41].

The clonal sectors of NSDHL negative cells that were visible in the fetal brain and retina of *Bpa*^{1H} embryos demonstrated that mutant progenitor cells were able to proliferate, migrate and begin to differentiate morphologically. This raises the question as to what extent these cells are able to differentiate and function relative to WT cells. Further studies that employ cell type specific markers and functional assays will be required to resolve this question in various tissues.

The liver provided a convenient organ in which to measure the long term survival of mutant cells in the *Bpa*^{1H} female. It comprises a relatively homogeneous population of hepatocytes that showed high expression of NSDHL at all stages of development, facilitating the quantitation of mutant and WT cells at different ages. The increased proportion of WT hepatocytes (79%) observed at one year of age relative to that at P6 (52%) suggests that the mutant cells are preferentially lost over the life of the adult animal. The nonrandom distribution of mutant and WT cells in the adult *Bpa*^{1H} liver, where WT cells preferentially occupy the pericentral region of the lobule, is consistent with the notion that mutant cell death accounts, at least in part, for the skewed ratio. Although it was once thought that hepatocyte proliferation is localized to the periportal region of the lobule and that cells migrate toward the pericentral

zone, more recent analyses that use cell lineage tracers and radiolabeling indicate that hepatocytes do not migrate in an organized pattern and that proliferation does not occur in a particular region of the lobule [42,43]. Thus, the nonrandom distribution of mutant and WT cells in the *Bpa*^{1H} adult liver is probably not caused by differential migration of the hepatocytes, although we cannot definitively exclude this model.

Another hypothesis is that mutant cells divide more slowly than WT cells in the pericentral region. If this were the case, we would expect to see patches of NSDHL negative cells similar to those in the pericentral region of the P25 liver present in this region of the older liver. Instead, mutant cells were virtually absent from the pericentral region in the older livers, and were usually found as individual cells or clusters smaller than in the P25 liver. Thus, we favor the hypothesis that the mutant cells die at a slightly higher rate in the pericentral region than in the periportal region of the lobule. This may be due to a greater accumulation of potentially cytotoxic sterol precursors caused by the *Bpa*^{1H} block to cholesterol biosynthesis in pericentral cells if they are programmed to synthesize cholesterol at a higher rate than periportal hepatocytes.

The apparent negative selection of mutant cells in the mosaic *Bpa*^{1H} liver was in contrast to our previous results that found no evidence of selection against the mutant cells in a mixed population of MEFs [20]. This discrepancy may be due to differences between fibroblasts in vitro and hepatocytes in vivo with regard to their rate of cholesterol biosynthesis, mechanisms of cholesterol efflux and import, or susceptibility to the possible deleterious effects of increased levels of sterol precursors. An understanding of why negative selection in the liver and other tissues is apparently more pronounced after birth than during embryogenesis will require additional experiments that investigate the role of maternal cholesterol in the development of *Bpa*^{1H} and wild type embryos.

Previous studies have shown that the skin is a site of significant cholesterol biosynthesis [30, 44]. In the stratum corneum of the epidermis, cholesterol is a one of several secreted lipids present in lamellar bodies that form a permeability barrier that prevents trans-epidermal water loss [45]. The source of the barrier cholesterol is thought to be mainly the epidermis and is independent of circulating cholesterol [46]. Mice that lack DHCR24, the enzyme that catalyzes the conversion of desmosterol to cholesterol, die within several hours after birth and show defects in the maturation of the epidermis, with compromised barrier function [47]. The skin of *Dhcr24* −/− pups is marked by hyperproliferation of immature keratinocytes. However, an inflammatory infiltrate in the dermis, such as that seen in the *Bpa*^{1H} skin, was not reported. Mice that lack DHCR7 also die within the first day of life, but have no reported skin abnormalities [4,6]. These results may reflect a difference in the ability of the sterol precursors desmosterol and 7-DHC to partially substitute for cholesterol in epidermal development and barrier function. Due to the perinatal lethality caused by these null alleles, their effect on hair follicle maturation is not known. However, some partially rescued *Dhcr7* −/− mice that carry a WT *Dhcr7* transgene under the control of the CNS-specific nestin promoter survive to P17 and have no reported skin or hair abnormalities [48].

Although barrier function was not tested in the skin of *Bpa*^{1H} mutants, we saw no gross morphological or histological abnormalities in the epidermis within NSDHL negative regions of the mosaic skin of pups at P2. The timing of the appearance of hyperkeratotic eruptions in *Bpa*^{1H} females at P6 coincided with the stage at which hair shafts emerge from the maturing follicles in WT skin. The strong expression of NSDHL seen in the maturing follicles, along with the short, immature appearance of hair follicles in the NSDHL negative areas of skin at P6 and in the 8 week old adult suggest that products from the endogenous cholesterol biosynthetic pathway are required for the completion of hair follicle development. Although the role of cholesterol biosynthesis in hair follicle development is not clear, it is known that

human hair follicles possess high HMGCR activity, at a level roughly 70% of that found in human liver cells [49]. Moreover, HMGCR activity in human hair follicles is not sensitive to either naturally occurring or experimentally induced changes in the level of exogenous LDL [49]. This suggests that, unlike many other tissues, hair follicles do not acquire cholesterol from plasma. Isolated apocrine and sebaceous glands, by contrast, show reduced HMGCR activity in response to the presence of exogenous cholesterol, indicating that they are able to take up plasma lipids [50]. The relative autonomy of hair follicles with regard to cholesterol synthesis may explain why, in affected *Bpa*^{1H} skin, they fail to develop fully, particularly in the cycling segment of the follicle where NSDHL expression is highest.

In the mouse, the brain roughly doubles in weight between 1 and 26 weeks of age. At the same time, the cholesterol content of the brain increases more than 6-fold [29]. The first three weeks after birth are marked by the highest rate of brain cholesterol synthesis. In the adult mouse, about 80% of the total brain cholesterol is in myelin that is synthesized by oligodendrocytes to provide insulating sheathes for neuronal axons and dendrites. While it is known that astrocytes synthesize cholesterol that is transported to neurons, the relative contribution of endogenous neuronal cholesterol biosynthesis vs transport from glial cells throughout development and maturation of the brain is not clear [51]. Previous studies have demonstrated that cultured neurons synthesize cholesterol [52]. Recently, it has been reported that de novo cholesterol biosynthesis in neurons is regulated by brain-derived neurotrophic factor (BDNF) and p75 neurotrophin receptor, based on changes in the expression levels of cholesterogenic enzymes [53,54]. In neurons, cholesterol-rich lipid rafts and caveolae are thought to play important roles in synaptogenesis and signal transduction that vary among different types of neurons [55,56].

Our analysis of the WT P2 brain showed that NSDHL is expressed at high levels in cortical neurons and the hippocampus. Consistent with the known decrease in the rate of cholesterol synthesis in mature animals, we observed both lower levels and a more restricted distribution of staining in the adult brain. The relatively broad sectors of NSDHL deficient cells, presumably including both neurons and glia, that were observed in the *Bpa*^{1H} brain at P2 suggest that these cells were able to acquire sufficient cholesterol by transport from WT cells to survive to birth. The apparent loss of these sectors in the adult mutant may be the result of negative selection during the period of high demand for cholesterol in the CNS during the first month of life, defects in synaptogenesis or prosurvival signaling, or the accumulation of toxic sterol intermediates due to the upregulation of the cholesterol biosynthetic pathway in the young adult. The lack of gross structural abnormalities in the *Bpa*^{1H} adult hippocampus implies that substantial numbers of cells may be lost between birth and maturity, although it is possible that some or all of these neurons may be replaced by proliferating neural progenitor cells that reside within the subgranular zone of the dentate gyrus and subventricular zone of the lateral ventricles [57]. Distinguishing between these possibilities and determining whether negative selection acts on all of the mutant cells in the *Bpa*^{1H} brain or only cells with a relatively high rate of endogenous cholesterol biosynthesis will require further investigation using conditional gene disruption approaches.

Supplementary Material

Refer to Web version on PubMed Central for supplementary material.

Acknowledgments

We thank Dr. Kim McBride for performing statistical analysis. This work was supported by NIH R01 HD38572 to G.E.H.

References

1. Simons K, Toomre D. Lipid rafts and signal transduction. Nat Rev Mol Cell Biol 2000;1:31–39. [PubMed: 11413487]
2. Ikonen E. Cellular cholesterol trafficking and compartmentalization. Nat Rev Mol Cell Biol 2008 Sep;: 125–138. [PubMed: 18216769]
3. Jeong J, McMahon AP. Cholesterol modification of Hedgehog family proteins. J Clin Invest 2002;110:591–596. [PubMed: 12208857]
4. Wassif CA, Zhu P, Kratz L, Krakowiak PA, Battaile KP, Weight FF, Grinberg A, Steiner RD, Nwokoro NA, Kelley RI, Stewart RR, Porter FD. Biochemical, phenotypic and neurophysiological characterization of a genetic mouse model of RSH/Smith--Lemli--Opitz syndrome. Hum Mol Genet 2001;10:555–564. [PubMed: 11230174]
5. Ohashi K, Osuga J, Tozawa R, Kitamine T, Yagyu H, Sekiya M, Tomita S, Okazaki H, Tamura Y, Yahagi N, Iizuka Y, Harada K, Gotoda T, Shimano H, Yamada N, Ishibashi S. Early embryonic lethality caused by targeted disruption of the 3-hydroxy-3-methylglutaryl-CoA reductase gene. J Biol Chem 2003;278:42936–42941. [PubMed: 12920113]
6. Fitzky BU, Moebius FF, Asaoka H, Waage-Baudet H, Xu L, Xu G, Maeda N, Kluckman K, Hiller S, Yu H, Batta AK, Shefer S, Chen T, Salen G, Sulik K, Simoni RD, Ness GC, Glossmann H, Patel SB, Tint GS. 7-Dehydrocholesterol-dependent proteolysis of HMG-CoA reductase suppresses sterol biosynthesis in a mouse model of Smith-Lemli-Opitz/RSH syndrome. J Clin Invest 2001;108:905–915. [PubMed: 11560960]
7. Herman GE. Disorders of cholesterol biosynthesis: prototypic metabolic malformation syndromes. Hum Mol Genet (No 1) 2003;12(Spec):R75–R88. [PubMed: 12668600]
8. Kelly DL, Rizzino A. DNA microarray analyses of genes regulated during the differentiation of embryonic stem cells. Mol.Reprod.Dev 2000;56:113–123. [PubMed: 10813842]
9. Waterham HR. Defects of cholesterol biosynthesis. FEBS Lett 580;2006:5442–5449.
10. Liu XY, Dangel AW, Kelley RI, Zhao W, Denny P, Botcherby M, Cattanach B, Peters J, Hunsicker PR, Mallon AM, Strivens MA, Bate R, Miller W, Rhodes M, Brown SD, Herman GE. The gene mutated in bare patches and striated mice encodes a novel 3beta-hydroxysteroid dehydrogenase. Nat Genet 1999;22:182–187. [PubMed: 10369263]
11. Caldas H, Herman GE. NSDHL, an enzyme involved in cholesterol biosynthesis, traffics through the Golgi and accumulates on ER membranes and on the surface of lipid droplets. Hum Mol Genet 2003;12:2981–2991. [PubMed: 14506130]
12. Phillips RJ, Hawker SG, Moseley HJ. Bare-patches, a new sex-linked gene in the mouse, associated with a high production of XO females. I. A preliminary report of breeding experiments. Genet Res 1973;22:91–99. [PubMed: 4588955]
13. Caldas H, Cunningham D, Wang X, Jiang F, Humphries L, Kelley RI, Herman GE. Placental defects are associated with male lethality in bare patches and striated embryos deficient in the NAD(P)H Steroid Dehydrogenase-like (NSDHL). Enzyme Mol Genet Metab 2005;84:48–60.
14. Emami S, Hanley KP, Esterly NB, Daniallinia N, Williams ML. X-linked dominant ichthyosis with peroxisomal deficiency: an ultrastructural and ultracytochemical study of the Conradi-Hunermann syndrome and its murine homologue, the bare patches mouse. Arch.Dermatol 1994;130:325–336. [PubMed: 8129411]
15. Happle R, Phillips RJS, Roessner A, Junemann G. Homologous genes for X-linked chondrodysplasia punctata in man and mouse. Hum.Genet 1983;63:24–27.. [PubMed: 6682087]
16. Konig A, Happle R, Bornholdt D, Engel H, Grzeschik K-H. Mutations in the NSDHL gene, encoding a 3β-hydroxysteroid dehydrogenase, cause CHILD syndrome. Am J Med Genet 2000;90:339–346. [PubMed: 10710235]
17. Happle R, Koch H, Lenz W. The CHILD syndrome. Congenital hemidysplasia with ichthyosiform erythroderma and limb defects. Eur.J.Pediatr 1980;134:27–33. [PubMed: 7408908]
18. Grange DK, Kratz LE, Braverman N, Kelley RI. CHILD syndrome caused by deficiency of 3β-hydroxysteroid-Δ^8, Δ^7-isomerase. Am.J.Med.Genet 2000;90:328–335. [PubMed: 10710233]

19. Dietschy JM, Turley SD. Thematic review series: brain Lipids. Cholesterol metabolism in the central nervous system during early development and in the mature animal. J Lipid Res 2004;45:1375–1397. [PubMed: 15254070]
20. Cunningham D, Swartzlander D, Liyanarachchi S, Davuluri RV, Herman GE. Changes in gene expression associated with loss of function of the NSDHL sterol dehydrogenase in mouse embryonic fibroblasts. J Lipid Res 2005;46:1150–1162. [PubMed: 15805545]
21. Mroz K, Hassold TJ, Hunt PA. Meiotic aneuploidy in the XXY mouse: evidence that a compromised testicular environment increases the incidence of meiotic errors. Hum Reprod 1999;14:1151–1156. [PubMed: 10325252]
22. Angel T, Faust C, Gonzales JC, Kenwrick S, Lewis RA, Herman GE. Genetic mapping of the X-linked dominant mutations striated (*Str*) and bare patches (*Bpa*) to a 600-kb region of the mouse X Chromosome: implications for mapping human disorders in Xq28. Mamm. Genome 1993;4:171–176. [PubMed: 8439729]
23. Vallejo CG, Seguido AM, Testillano PS, Risueno MC. Thyroid hormone regulates tubulin expression in mammalian liver. Effects of deleting thyroid hormone receptor-alpha or -beta. Am J Physiol Endocrinol Metab 2005;289:E87–E94. [PubMed: 15713690]
24. Schneider MR, Schmidt-Ullrich R, Paus R. The hair follicle as a dynamic miniorgan. Curr Biol 2009;19:R132–R142. [PubMed: 19211055]
25. O'Shaughnessy RF, Christiano AM. Inherited disorders of the skin in human and mouse: from development to differentiation. Int J Dev Biol 2004;48:171–179. [PubMed: 15272382]
26. Bol DK, Rowley RB, Ho CP, Pilz B, Dell J, Swerdel M, Kiguchi K, Muga S, Klein R, Fischer SM. Cyclooxygenase-2 overexpression in the skin of transgenic mice results in suppression of tumor development. Cancer Res 2002;62:2516–2521. [PubMed: 11980643]
27. Waikel RL, Kawachi Y, Waikel PA, Wang XJ, Roop DR. Deregulated expression of c-Myc depletes epidermal stem cells. Nat Genet 2001;28:165–168. [PubMed: 11381265]
28. Dietschy JM, Turley SD. Cholesterol metabolism in the brain. Curr Opin Lipidol 2001;12:105–112. [PubMed: 11264981]
29. Quan G, Xie C, Dietschy JM, Turley SD. Ontogenesis and regulation of cholesterol metabolism in the central nervous system of the mouse. Brain Res Dev Brain Res 2003;146:87–98.
30. Turley SD, Andersen JM, Dietschy JM. Rates of sterol synthesis and uptake in the major organs of the rat in vivo. J Lipid Res 1981;22:551–569. [PubMed: 7276735]
31. Spady DK, Dietschy JM. Sterol synthesis in vivo in 18 tissues of the squirrel monkey, guinea pig, rabbit, hamster, and rat. J Lipid Res 1983;24:303–315. [PubMed: 6842086]
32. Shrivastava S, Paila YD, Dutta A, Chattopadhyay A. Differential effects of cholesterol and its immediate biosynthetic precursors on membrane organization. Biochemistry 2008;47:5668–5677. [PubMed: 18442257]
33. Vainio S, Jansen M, Koivusalo M, Rog T, Karttunen M, Vattulainen I, Ikonen E. Significance of sterol structural specificity. Desmosterol cannot replace cholesterol in lipid rafts. J Biol Chem 2006;281:348–355. [PubMed: 16249181]
34. Jansen M, Pietiainen VM, Polonen H, Rasilainen L, Koivusalo M, Ruotsalainen U, Jokitalo E, Ikonen E. Cholesterol substitution increases the structural heterogeneity of caveolae. J Biol Chem 2008;283:14610–14618. [PubMed: 18353778]
35. Tozawa R, Ishibashi S, Osuga J, Yagyu H, Oka T, Chen Z, Ohashi K, Perrey S, Shionoiri F, Yahagi N, Harada K, Gotoda T, Yazaki Y, Yamada N. Embryonic lethality and defective neural tube closure in mice lacking squalene synthase. J Biol Chem 1999;274:30843–30848. [PubMed: 10521476]
36. Krakowiak PA, Wassif CA, Kratz L, Cozma D, Kovarova M, Harris G, Grinberg A, Yang Y, Hunter AG, Tsokos M, Kelley RI, Porter FD. Lathosterolosis: an inborn error of human and murine cholesterol synthesis due to lathosterol 5-desaturase deficiency. Hum Mol Genet 2003;12:1631–1641. [PubMed: 12812989]
37. Laubner D, Breitling R, Adamski J. Embryonic expression of cholesterogenic genes is restricted to distinct domains and colocalizes with apoptotic regions in mice. Brain Res Mol Brain Res 2003;115:87–92. [PubMed: 12824059]
38. Tint GS, Yu H, Shang Q, Xu G, Patel SB. The use of the Dhcr7 knockout mouse to accurately determine the origin of fetal sterols. J Lipid Res 2006;47:1535–1541. [PubMed: 16651660]

39. Yoshida S, Wada Y. Transer of maternal cholesterol to embryo and fetus in pregnant mice. J Lipid Res 2005;46:2168–2174. [PubMed: 16061954]
40. Guarneri P, Guarneri R, Cascio C, Pavasant P, Piccoli F, Papadopoulos V. Neurosteroidogenesis in rat retinas. J Neurochem 1994;63:86–96. [PubMed: 7911514]
41. Compagnone NA, Bulfone A, Rubenstein JL, Mellon SH. Expression of the steroidogenic enzyme P450scc in the central and peripheral nervous systems during rodent embryogenesis. Endocrinology 1995;136:2689–2696. [PubMed: 7750493]
42. Magami Y, Azuma T, Inokuchi H, Kokuno S, Moriyasu F, Kawai K, Hattori T. Cell proliferation and renewal of normal hepatocytes and bile duct cells in adult mouse liver. Liver 2002;22:419–425. [PubMed: 12390477]
43. Bralet MP, Branchereau S, Brechot C, Ferry N. Cell lineage study in the liver using retroviral mediated gene transfer. Evidence against the streaming of hepatocytes in normal liver. Am J Pathol 1994;144:896–905. [PubMed: 8178942]
44. Feingold KR, Brown BE, Lear SR, Moser AH, Elias PM. Localization of de novo sterologenesis in mammalian skin. J Invest Dermatol 1983;81:365–369. [PubMed: 6619567]
45. Feingold KR. Thematic review series: skin lipids. The role of epidermal lipids in cutaneous permeability barrier homeostasis. J Lipid Res 2007;48:2531–2546. [PubMed: 17872588]
46. Andersen JM, Dietschy JM. Regulation of sterol synthesis in 15 tissues of rat. II. Role of rat and human high and low density plasma lipoproteins and of rat chylomicron remnants. J Biol Chem 1977;252:3652–3659. [PubMed: 193842]
47. Mirza R, Hayasaka S, Takagishi Y, Kambe F, Ohmori S, Maki K, Yamamoto M, Murakami K, Kaji T, Zadworny D, Murata Y, Seo H. DHCR24 gene knockout mice demonstrate lethal dermopathy with differentiation and maturation defects in the epidermis. J Invest Dermatol 2006;126:638–647. [PubMed: 16410790]
48. Yu H, Wessels A, Tint GS, Patel SB. Partial rescue of neonatal lethality of Dhcr7 null mice by a nestin promoter-driven DHCR7 transgene expression. Brain Res Dev Brain Res 2005;156:46–60.
49. Brannan PG, Goldstein JL, Brown MS. 3-hydroxy-3-methylglutaryl coenzyme A reductase activity in human hair roots. J Lipid Res 1975;16:7–11. [PubMed: 162931]
50. Smythe CD, Greenall M, Kealey T. The activity of HMG-CoA reductase and acetyl-CoA carboxylase in human apocrine sweat glands, sebaceous glands, and hair follicles is regulated by phosphorylation and by exogenous cholesterol. J Invest Dermatol 1998;111:139–148. [PubMed: 9665401]
51. Pfrieger FW. Outsourcing in the brain: do neurons depend on cholesterol delivery by astrocytes? Bioessays 2003;25:72–78. [PubMed: 12508285]
52. Vance JE, Campenot RB, Vance DE. The synthesis and transport of lipids for axonal growth and nerve regeneration. Biochim Biophys Acta 2000;1486:84–96. [PubMed: 10856715]
53. Korade Z, Mi Z, Portugal C, Schor NF. Expression and p75 neurotrophin receptor dependence of cholesterol synthetic enzymes in adult mouse brain. Neurobiol Aging 2007;28:1522–1531. [PubMed: 16887237]
54. Suzuki S, Kiyosue K, Hazama S, Ogura A, Kashihara M, Hara T, Koshimizu H, Kojima M. Brain-derived neurotrophic factor regulates cholesterol metabolism for synapse development. J Neurosci 2007;27:6417–6427. [PubMed: 17567802]
55. Korade Z, Kenworthy AK. Lipid rafts, cholesterol, and the brain. Neuropharmacology 2008;55:1265–1273. [PubMed: 18402986]
56. Ko M, Zou K, Minagawa H, Yu W, Gong JS, Yanagisawa K, Michikawa M. Cholesterol-mediated neurite outgrowth is differently regulated between cortical and hippocampal neurons. J Biol Chem 2005;280:42759–42765. [PubMed: 16267051]
57. Zhao C, Deng W, Gage FH. Mechanisms and functional implications of adult neurogenesis. Cell 2008;132:645–660. [PubMed: 18295581]

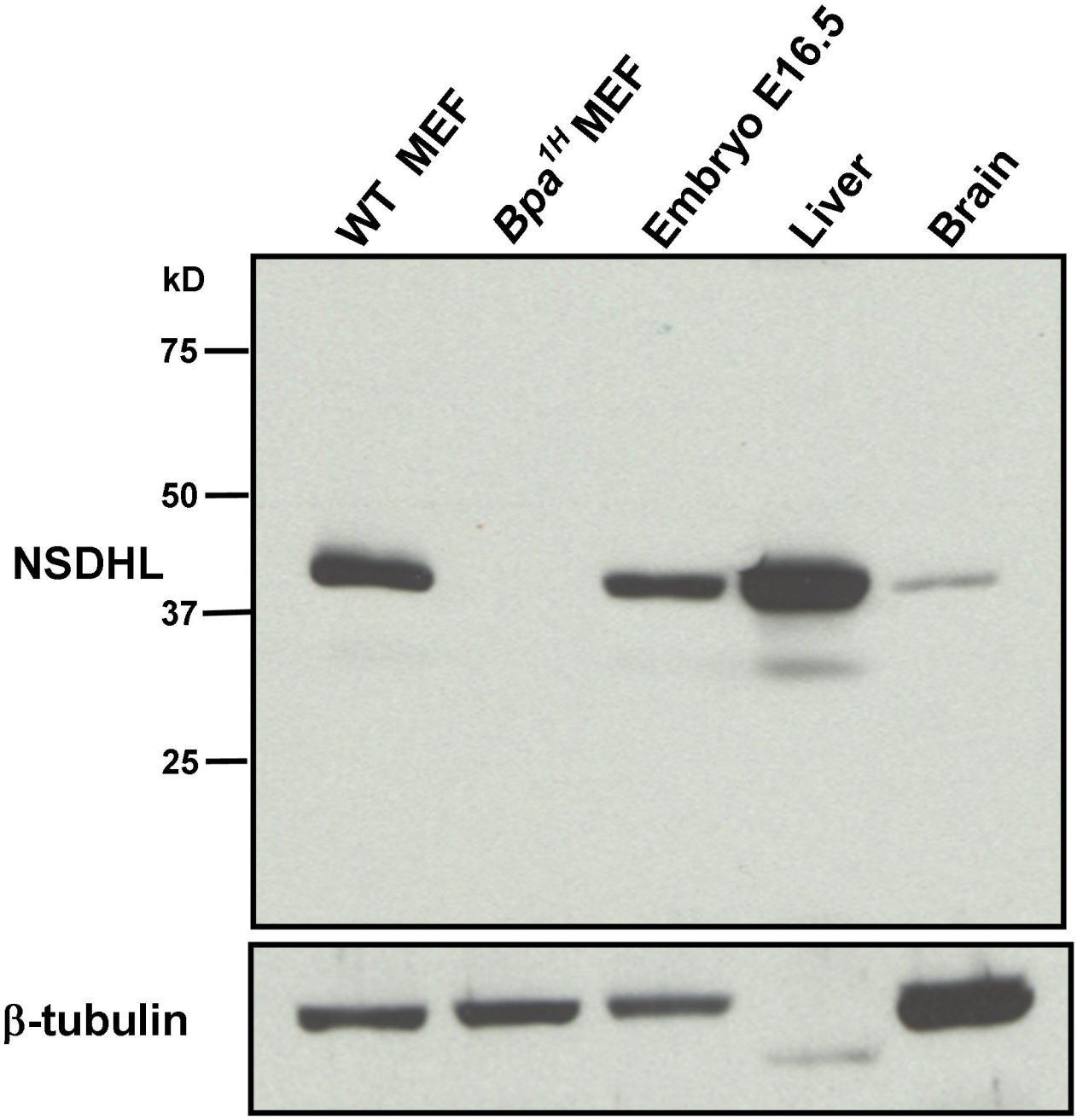

Figure 1. Detection of NSDHL in whole protein extracts by Western blot analysis using a purified anti-NSDHL polyclonal antibody

Approximately 10 μg of total protein from WT and *Bpa*^{1H} MEFs, WT E16.5 embryo, 7 mo WT female liver and 7 mo WT female brain were resolved by PAGE, transferred to nylon membrane and probed with a polyclonal anti-NSDHL antibody at a 1:4000 dilution. Antibody binding was visualized by chemiluminescence detection (see methods). A single prominent band that migrated slightly above the 37 kD marker was detected in all samples except the *Bpa*^{1H} MEF. A duplicate blot was probed with an anti-β-tubulin antibody to verify the presence of intact protein in the extracts.

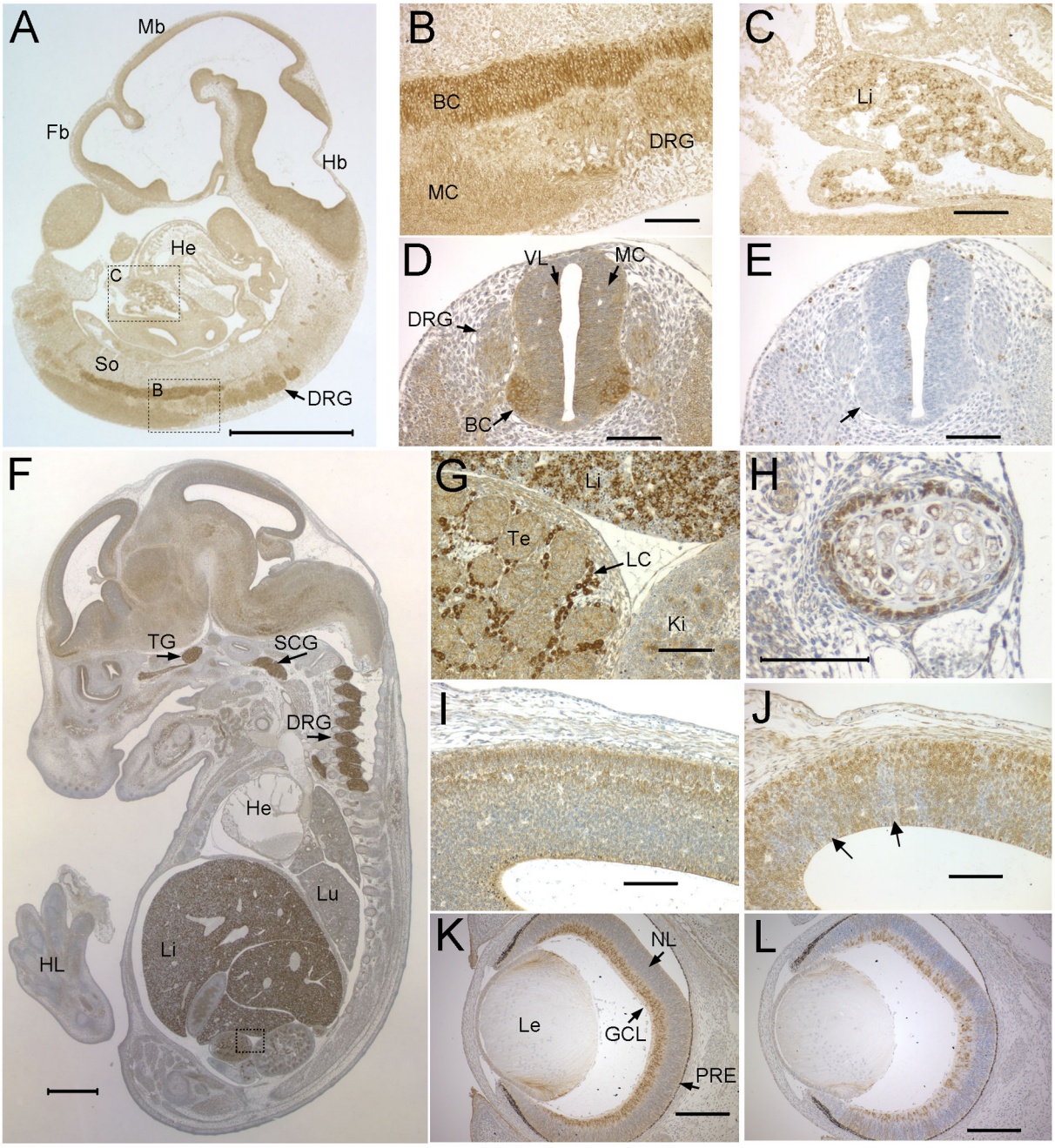

Figure 2. Developmental expression pattern of NSDHL in mouse embryos

A. A saggital section from an E10.5 WT embryo immunostained for NSDHL showed the highest signal in the CNS and fetal liver. **B.** A higher magnification view of boxed area B in panel A showing intense staining of the basal column (BC) of the neural tube, with less signal in the mantle column (MC) and caudal dorsal root ganglia (DRG). **C.** A higher magnification view of boxed area C in panel A showing a subpopulation of strongly stained cells in the fetal liver (Li). **D.** A transverse section through the posterior neural tube illustrates the high level of NSDHL staining in the basal column of the neural tube relative to the mantle column and ventricular layer (VL). **E.** A section adjacent to that shown in panel D immunostained for phosphorylated histone H3, that marks mitotic cells, shows numerous dividing cells in the

ventricular layer lining the neural tube, with no positive cells in the basal column, where the strongest NSDHL signal is seen (arrow). **F.** A saggital section from an E14.5 WT embryo immunostained for NSDHL shows intense staining in the liver, dorsal root ganglia, and trigeminal ganglion (TG). Signal in the brain is higher than in other tissues such as heart (He) and lung (Lu). **G.** A high magnification view of the boxed area from panel F, showing strong staining of the Leydig cells (LC) in the testis, comparable to the level in hepatocytes seen in the adjacent fetal liver. **H.** High magnification view of developing rib from section shown in panel F. NSDL staining is seen in cells of the condensing mesenchyme surrounding the chondrocytes of the rib. **I.** A high magnification view of the posterior neopallial cortex of the brain from the section shown in panel F. **J.** The same region of the brain shown in panel I from a *Bpa*^{1H} E14.5 female embryo was immunostained for NSDHL. Note the patchy staining pattern, with radiating sectors of neurons showing no staining (arrows). **K.** A transverse section through the eye of a WT E15.5 embryo showing strong NSDHL staining in the ganglion cell layer (GCL). **L.** NSDHL staining of a *Bpa*^{1H} E15.5 eye, showing mosaic expression in the GCL with radiating sectors of NSDHL positive and negative cells in progeny cells of the developing retina. Sections in panels B–L were lightly counterstained with hematoxylin. The size bars in panels A and F represent 1 mm. Size bars in all other panels denote 100 μm. Abbreviations: BC, basal column; DRG, dorsal root ganglion; Fb, forebrain; GCL, ganglion cell layer; Hb, hindbrain; He, heart; HL, hind limb; Ki, kidney; LC, Leydig cell; Le, lens; Lu, lung; Mb, midbrain; MC, mantle column; NL, neuroblast layer; PRE, pigmented retinal epithelium; VL, ventricular layer.

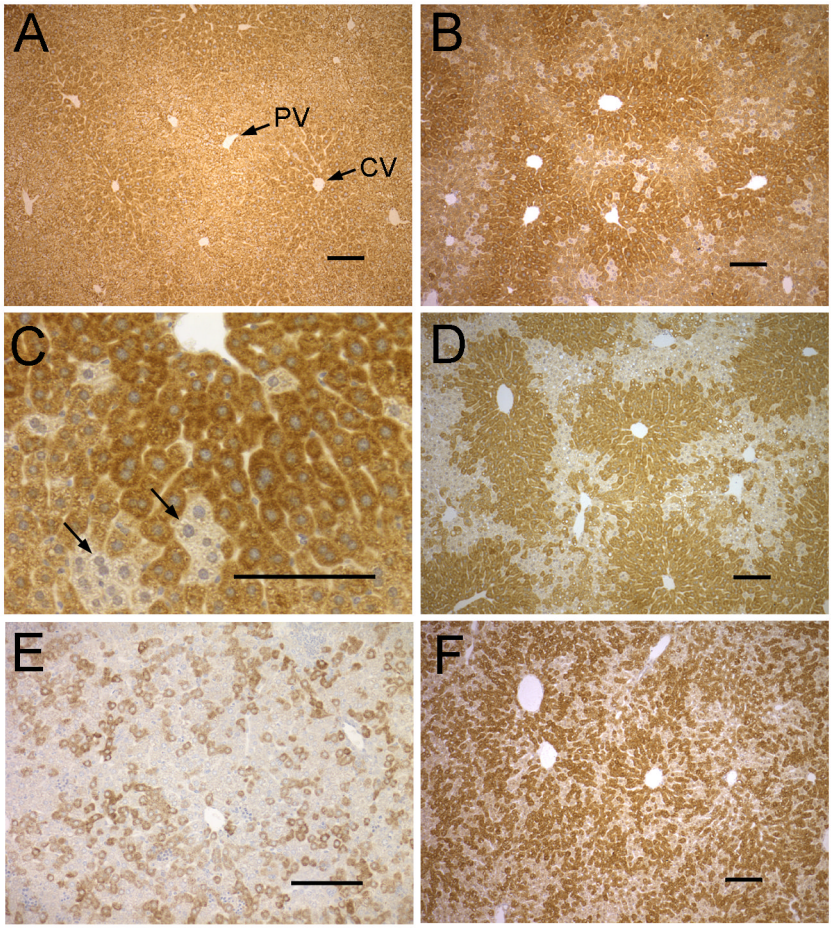

Figure 3. Immunostaining of NSDHL in WT and *Bpa*^{1H} liver

A. Adult (3 mo) WT liver shows strong staining thoughout the lobule, with slightly higher signal in the pericentral region. **B.** An adult (13 mo) *Bpa*^{1H} liver with a large majority of NSDHL positive cells. **C.** A high magnification view of the liver shown in panel B showing small clusters of hepatocytes that did not stain for NSDHL. **D.** An adult (13 mo) *Bpa*^{1H} liver with a relatively large number of NSDHL negative hepatocytes. Note the high proportion of NSDHL positive cells surrounding the central veins. NSDHL staining in the liver of a P6 *Bpa*^{1H} female. **F.** NSDHL staining in the liver of a P25 *Bpa*^{1H} female. Abbreviations: CV, central vein; PV, portal vein. Size bars represent 100 μm.

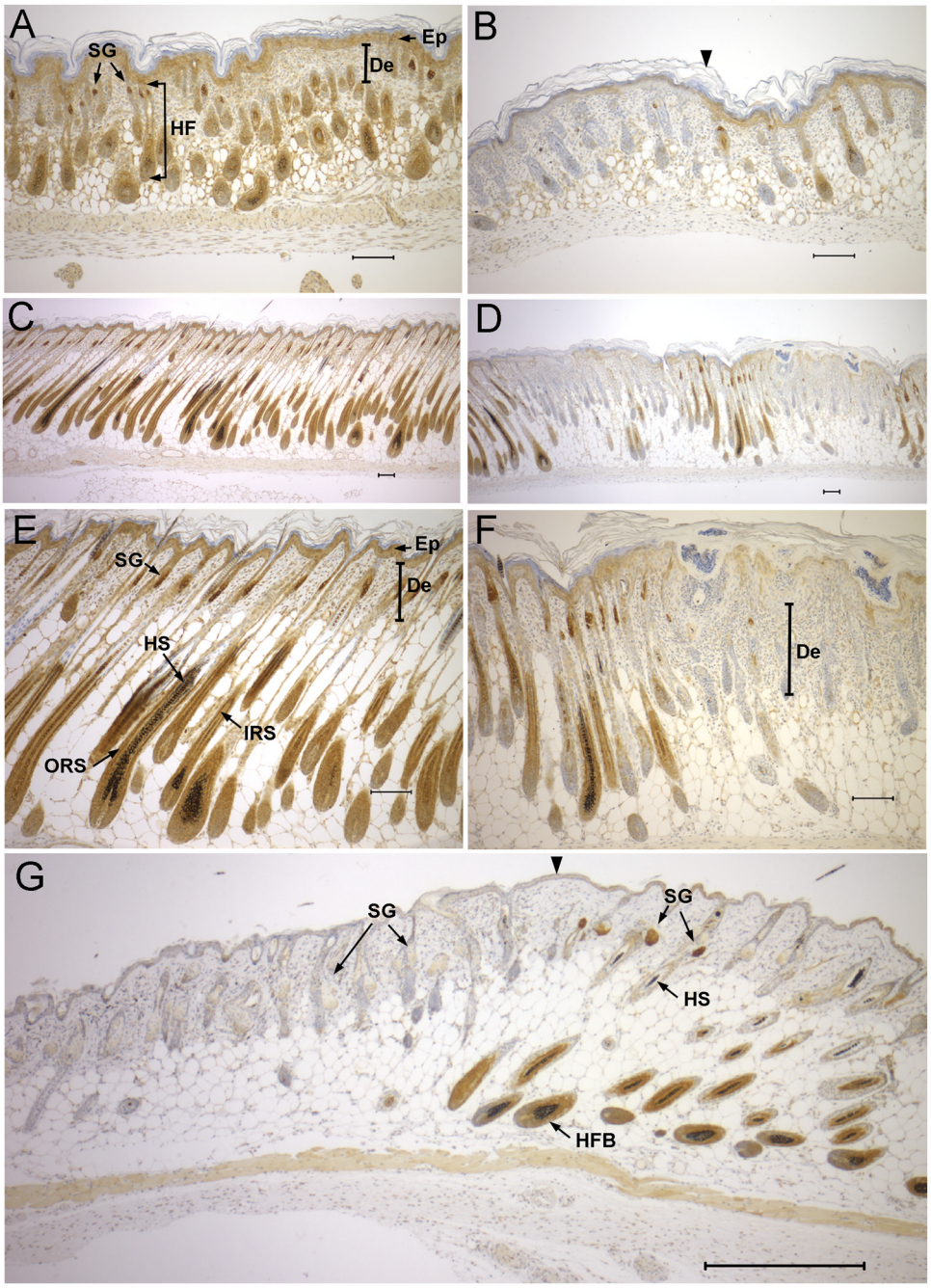

Figure 4. NSDHL expression in developing dorsal skin and hair follicles

A. NSDHL staining in dorsal skin of a P2 WT pup shows strong signal in the sebaceous glands, and expression in the inner root sheath of the developing hair follicle, as well as the epidermis. **B.** In dorsal skin of a *Bpa*^{1H} P2 pup, regions lacking detectable NSDHL in the epidermis and developing hair follicles (left of arrowhead) appeared similar histologically to regions that stained positively for NSDHL (right of arrowhead). **C.** WT skin from P6 displayed strong NSDHL staining in the outer root sheath and moderate staining in the inner root sheath of the maturing hair follicle. **D.** In *Bpa*^{1H} skin at P6, NSDHL negative regions showed a thickening of the epidermis and dermis with developmentally delayed hair follicles. **E.** Higher magnification view of the sample shown in panel C. **F.** Higher magnification of the sample

shown in panel D. **G.** NSDHL staining in dorsal skin of a *Bpa*^{1H} female at 8 weeks of age. Strong staining in sebaceous glands and the inner root sheath of anagen stage hair follicles is visible in the region to the right of the arrowhead. The area on the left shows virtually no staining in the enlarged sebaceous glands and mainly telogen stage hair follicles. No hair shafts are present within the hair follicles in this region. Abbreviations: De, dermis; Ep, epidermis; HF, hair follicle; HFB, hair follicle bulb; HS, hair shaft; IRS, inner root sheath; ORS, outer root sheath; SG, sebaceous gland. Size bars represent 100 μm.

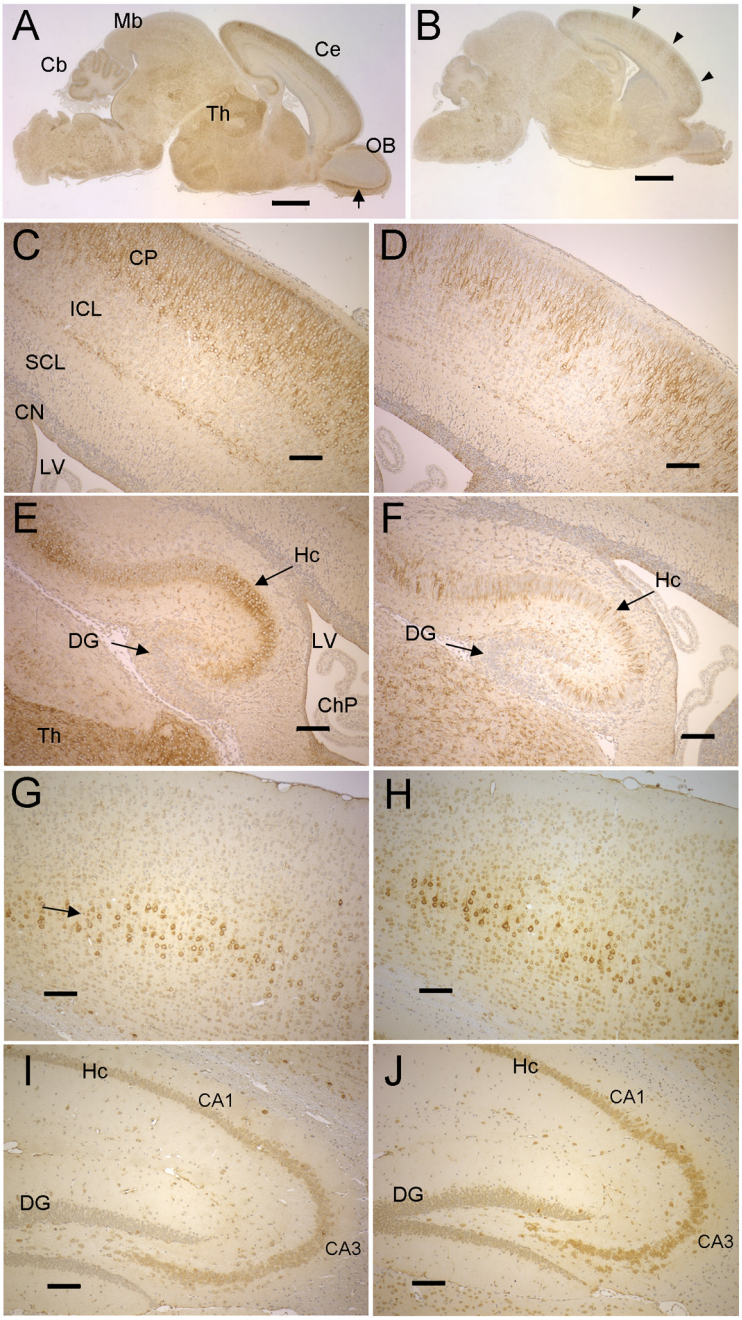

Figure 5. NSDHL in early postnatal and adult brains of WT and *Bpa*^{1H} females

A. NSDHL staining of a saggital section from a WT P2 brain. The arrow indicates the mitral layer of the olfactory bulb. **B.** NSDHL staining of a *Bpa*^{1H} P2 brain. Arrowheads indicate radial sectors of low NSDHL signal in the cerebrum. **C.** A higher magnification of the cerebral cortex from the section shown in panel A shows a broad, even band of positively stained pyramidal neurons in the outer layer of the cortex. **D.** A higher magnification of the cerebral cortex from the *Bpa*^{1H} brain section shown in panel B reveals regions of unstained cortical neurons that were not seen in the WT brain. **E.** A higher magnification of the hippocampus (Hc) from the WT brain shown in panel A. **F.** High magnification of the hippocampus from the *Bpa*^{1H} brain shown in panel B, showing a mosaic pattern of NSDHL within the hippocampus. **G.** NSDHL

staining in the cerebral cortex on a saggital section of a WT adult brain. The arrow indicates a layer of relatively large pyramidal neurons that showed the highest level of NSDHL signal in the adult cerebral cortex. **H.** NSDHL staining in the cerebral cortex of a *Bpa*^{1H} adult brain. **I.** NSDHL staining in the hippocampus of a WT adult brain. **J.** NSDHL staining in the hippocampus of a *Bpa*^{1H} adult brain. Abbreviations: Cb, cerebellum; Ce, cerebrum; ChP, choroid plexus; CN, cortical neurepithelium; CP, cortical plate; Cx, cerebral cortex; DG, dentate gyrus; Hc, hippocampus; Ht, hypothalamus; ICL, intermediate cortical layer; LV, lateral ventricle; OB, olfactory bulb; SCL, subventricular cortical layer; Th, thalamus. Size bars in panels A and B correspond to 1 mm. Size bars in panels C–J correspond to 100 μm.